Front. Phys. 13(4), 134206 (2018)
https://doi.org/10.1007/s11467-018-0781-3

RESEARCH ARTICLE

Negative refraction based on purely imaginary metamaterials

Yang-Yang Fu[1,2], Ya-Dong Xu[2,†], Huan-Yang Chen[1,‡]

[1] *Institute of Electromagnetics and Acoustics and Department of Electronic Science, Xiamen University, Xiamen 361005, China*
[2] *College of Physics, Optoelectronics and Energy, Soochow University, Suzhou 215006, China*
Corresponding authors. E-mail: †ydxu@suda.edu.cn, ‡kenyon@xmu.edu.cn
Received January 20, 2018; accepted February 8, 2018

By introducing a new mechanism based on purely imaginary metamaterials (PIMs), we reveal that bidirectional negative refraction and planar focusing can be obtained using a pair of PIM slabs, overcoming the unidirectional limit in parity-time (PT)-symmetric systems. Compared with PT-symmetric systems, which require two different types of materials, the proposed negative refraction can be realized using two identical media. In addition, asymmetric excitation with bidirectional total transmission is observed in our PIM system. Therefore, a new way to realize negative refraction with properties that are unavailable in PT-symmetric systems is presented.

Keywords negative refraction, coherent perfect absorber, laser, purely imaginary metamaterials

PACS numbers 42.15.Eq, 42.25.Kb, 42.30.Va

1 Introduction

In optics, refraction of light at an interface of two different homogeneous media is a significant phenomenon playing important roles in many optical devices. According to Snell's law, for two conventional materials with positive refractive indices, the refracted light has the same direction as the incident one. The behavior is therefore called positive refraction. When one of the two materials is replaced by a negative-index one, the refracted light has the opposite direction from the incident one, i.e., negative refraction occurs [1]. In the past few years, negative refraction has attracted much attention because of its numerous intriguing applications, including the perfect lens [2], reversed Cherenkov radiation [3], and the negative Goos–Hänchen shift [4]. Various schemes to realize negative refraction have been proposed, such as the use of metamaterials [5–8], photonic crystals [9, 10], gradient gratings [11, 12], phase-conjugating surfaces [13, 14], and nonlinear optical films [15, 16]. Each of these approaches has advantages for negative refraction, but they are all found experimentally and theoretically to be imperfect because their performance is largely limited by the inherent loss. Therefore, negative refraction remains an unsolved issue, and other strategies, in particular those based on new mechanisms, are extremely desirable.

Parity-time (PT)-symmetric systems [17–25] provide a new approach. Recently, negative refraction was theoretically demonstrated in a pair of PT-symmetric metasurfaces [26]. One is a gain layer, and the other is a loss layer; they are separated by an air gap [see Fig. 1(b)], and both layers exhibit PT symmetry. When the PT-symmetric system is at the exceptional point [27, 28], negative refraction is observed for waves incident at a specific angle from the loss side. The underlying physics rests on the fact that coherent perfect absorber (CPA) and laser modes can occur in the loss and gain media, respectively, with unidirectional energy flow from the gain medium to the loss medium [see the black arrow in Fig. 1(b)]. In contrast to other solutions, loss-free and wide-angle negative refraction can be realized in PT-symmetric systems without bulk metamaterials or nonlinear effects. However, this working principle of negative refraction is inapplicable for waves incident from the gain side, because CPA and laser modes are not supported in the gain and loss media, respectively. Therefore, there is a unidirectional limit in PT-symmetric systems.

Conjugate metamaterials (CMs) [29–35] have recently drawn much attention as a type of non-Hermitian material. In CMs, the phases of permittivity and permeabil-

*arXiv: 1708.02358.

ity are complex conjugates of each other, for instance, $\varepsilon = |\varepsilon|\exp(-\mathrm{i}\alpha)$ and $\mu = |\mu|\exp(\mathrm{i}\alpha)$. By employing a CM slab, a perfect lens was demonstrated as a limited case for CMs with $\alpha = \pi$ [33]. In particular, when $\alpha = \pi/2$, such CMs are purely imaginary, and we defined the corresponding CMs as purely imaginary metamaterials (PIMs) [34], which are described by $\varepsilon = -\mathrm{i}|\varepsilon|$ and $\mu = \mathrm{i}|\mu|$ with $\varepsilon = \mu$ or $\varepsilon \neq \mu$. We also found that the CPA and laser modes (and even their coexistence) can be found in a PIM slab [34]. Therefore, PIMs might be used to achieve negative refraction by a mechanism similar to that of negative refraction in PT-symmetric systems, overcoming the disadvantages of both bulk metamaterials (inherent loss) and PT-symmetric systems (unidirectional limit). The aim of this work is to reveal a new strategy based on PIMs for realizing negative refraction. We systematically and thoroughly investigate a system of two PIM layers separated by an air gap [see Fig. 1(b)]. We show that (i) for PIMs in which the CPA and laser modes function under different conditions, asymmetrically perfect negative refraction appears; perfect negative refraction is obtained for incident waves from one side, whereas for incident waves from the other side, imperfect negative refraction with scattering appears. To some extent, such results are beyond the unidirectional limit of negative refraction in PT-symmetric systems. (ii) When the CPA and laser modes operate simultaneously in PIMs, perfect bidirectional negative refraction can be realized using only a pair of identical PIMs, which is a step toward the outcomes from PT-symmetric systems. (iii) In particular, if the refractive indices of the PIMs are less than unity, the negative refraction will disappear. Instead, asymmetric electromagnetic excitation occurs in the air gap, although bidirectional total transmission appears. (iv) Furthermore, bidirectional negative refraction and planar focusing [36] are well demonstrated in more generalized PIMs with subwavelength thicknesses. In fact, negative refraction in PIM systems is also loss-free and wide-angle, because it has the same working principle as that in PT-symmetric systems. Therefore, our proposed PIM systems show more interesting phenomena as well as underlying physics.

2 Analytical results

Before further discussion, let us revisit the CPA and laser effects in a PIM slab in air [34]. As shown in Fig. 1(a), in a so-called CPA, two coherent incident waves are totally absorbed in a PIM slab without any reflection (see the blue dashed arrows). In contrast, for incident waves without coherence, a laser mode with two intense outgoing waves will be generated, as indicated by the red

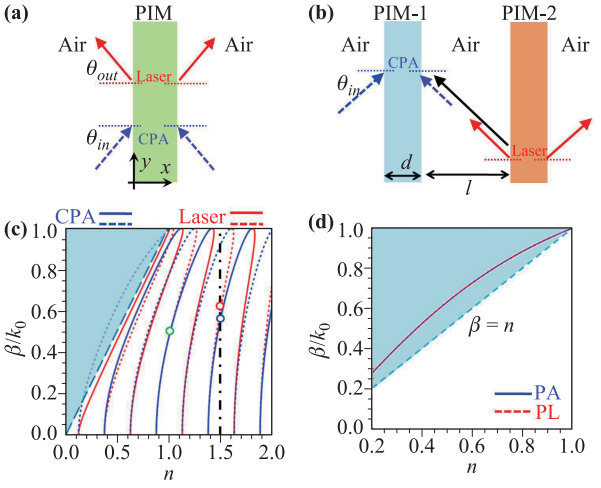

Fig. 1 **(a)** A schematic diagram of CPA and laser modes in a PIM slab. **(b)** A schematic diagram of negative refraction using PIMs. **(c)** is the dispersion relationship (β vs. n) of CPA modes (the blue curves) and laser modes (the red curves) for PIM-1 with $\varepsilon = \mu = n$. The corresponding solid and dashed curves are even and odd modes, respectively. The dashed line inside the color region is the critical angle for a PIM slab. The green point denotes the coexistence of CPA and laser modes for $n = 1$; the blue and red points represent that CPA and laser modes happen at different tangential momenta for $n = 1.5$. **(d)** is the dispersion relationship (β vs. n) of PA modes (the blue solid curve) for PIM-1with $\varepsilon = \mu = n$ and PL modes (the red dashed curves) for PIM-2 with $\varepsilon = \mu = n$. In all the calculations $d = 2\lambda$.

solid arrows in Fig. 1(a). These CPA and laser modes in PIMs can also lead to negative refraction. A schematic diagram of the fundamental principle for realizing negative refraction is shown in Fig. 1(b), where two PIM slabs of thickness d are separated by an air gap of length l. If the left and right PIM slabs support the CPA and laser modes, respectively, backward energy flow [see the black arrow in Fig. 1(b)] can occur in the air gap for waves incident from the left side, causing negative refraction. In this process, the left incident wave and the unidirectional wave (the black arrow) in the air gap are coherent, and their phases at the left PIM interface are determined by the properties of the CPA modes [34] (i.e., whether they are in phase or out of phase); the transmitted wave and unidirectional wave in the air gap are also coherent, and their phases at the right PIM interface depend on the properties of the laser modes [34] (whether they are in phase or out of phase). Therefore, for waves incident from the left in a fixed PIM structure (where the phase accumulation in the air gap is also fixed), the unidirectional and transmitted waves are also well-defined. As the loss and gain elements are both included in PIMs, the right and left PIM slabs can also support CPA and laser modes, respectively. Likewise, following a process

similar to that for left incidence, negative refraction can occur under right incidence, and bidirectional negative refraction can be realized in our PIM system.

To realize negative refraction in a PIM system, the conditions of the CPA and laser modes must be addressed; they can be obtained by analyzing the wave scattering of a PIM slab. We first study a single PIM slab (PIM-1) with parameters $\varepsilon_1 = -\mathrm{i}\varepsilon$ and $\mu_1 = \mathrm{i}\mu$, where ε and μ are positive numbers. We consider a transverse electric (TE) polarized wave with the electric field only along the z direction. After eigenmode analysis, the dispersion relationships for the CPA and laser modes are [34]

$$\eta_1 = -\mathrm{i}\sigma \cot(k_{1x}d/2) \text{ (odd)}, \tag{1a}$$

$$\eta_1 = \mathrm{i}\sigma \tan(k_{1x}d/2) \text{ (even)}, \tag{1b}$$

where $\eta_1 = k_x\mu_1/k_{1x}$, with $k_x = (k_0^2 - \beta^2)^{1/2}$ and $k_{1x} = (n_1^2k_0^2 - \beta^2)^{1/2}$ ($n_1^2 = n^2 = \varepsilon\mu$); k_0 and β are the wave vector in air and the y component of the propagating wave vector (tangential momentum), respectively; and $\sigma = 1$ for laser mode, whereas $\sigma = -1$ for CPA mode. Even modes are defined as symmetric modes, i.e., the field distribution in the x direction is symmetric. Odd modes are antisymmetric modes, i.e., the field distribution in the x direction is antisymmetric. Note that the CPA mode is the time-reversed counterpart of the laser mode, which is applicable in PIMs. Therefore, if there is another PIM slab with $\varepsilon_2 = \mathrm{i}\varepsilon$ and $\mu_2 = -\mathrm{i}\mu$ (PIM-2), we can also find the CPA and laser modes. As PIM-2 is the time-reversed form of PIM-1, for a single PIM-2 slab, $\sigma = 1$ and $\sigma = -1$ in Eq. (1) are related to the CPA and laser modes, respectively. In other words, if we obtain the CPA (laser) mode in a PIM-1 slab, the laser (CPA) mode will be realized in a PIM-2 slab.

For simplicity, $\varepsilon = \mu = n$ is set for PIMs to investigate the significant CPA and laser modes (similar results will still be obtained for PIMs with $\varepsilon \neq \mu$). On the basis of Eq. (1), Fig. 1(c) analytically shows the dispersion relationships $\beta(n)$ for CPA modes (the blue curves) and laser modes (the red curves) for the PIM-1 ($\varepsilon = \mu = n$) slab with $d = 2\lambda$ (where λ is the working wavelength), in which the solid and dashed curves correspond to the even and odd modes, respectively. For PIM-2 ($\varepsilon = \mu = n$), the red and blue curves in Fig. 1(c) correspond to the CPA and laser modes, respectively. Note that studies of the CPA and laser modes in PIM-1 and their associated physics have been reported in Ref. [34]. Therefore, we use the relevant results and focus on how to realize the negative refraction effect using PIMs. Several main points must be recalled for further discussion. (i) A PIM slab of interest can support not only the CPA mode, but also the laser mode. In particular, both the CPA and laser modes can occur at the same $\beta(n)$ [e.g., $n = 1$; see the green point in Fig. 1(c)] or at different $\beta(n)$ [e.g., $n = 1.5$; see the red and blue points in Fig. 1(c)], which is determined by the resonance conditions of the CPA and laser modes [33]. (ii) Specifically, for a lower refractive index ($0 < n < 1$), there is conventionally a critical angle $\theta_c = \arcsin(n)$ for total internal reflection. The critical angle for a PIM slab (marked by the dashed line inside the colored region) is shown in Fig. 1(c). Note that only the CPA or laser mode for PIMs can occur when the wave vector $\beta(n)$ is beyond its critical angle. Specifically, the PIM-1 slab can support only the CPA mode, and two coherent incoming waves for the CPA mode in the PIM-1 slab can be simplified to the case of a single incoming wave perfectly absorbed by it. This is because the two incoming coherent waves for the CPA mode will be bounded waves (or decayed waves) in the PIM slab, and they do not interact with each other owing to the shorter decay lengths; for more details, please see Ref. [34]. As coherent conditions are not required, we defined such modes as perfect absorber (PA) modes; their dispersion relationship is given as

$$\eta_1 = k_x\mu_1/k_{1x} = 1, \text{ with } k_{1x} = \mathrm{i}\sqrt{\beta^2 - n_1^2k_0^2}. \tag{2}$$

For a PIM-2 slab with a lower refractive index, only the laser mode can appear when the required momentum is beyond the critical angle. In this case, in contrast to the PA mode, a single incoming wave will be greatly enhanced in a PIM-2 slab without any reflection, which is defined as a perfect laser (PL) mode; the corresponding dispersion is

$$\eta_2 = k_x\mu_2/k_{2x} = -1, \text{ with } k_{2x} = \mathrm{i}\sqrt{\beta^2 - n_2^2k_0^2}. \tag{3}$$

Figure 1(d) shows these PA modes supported by PIM-1 with $\varepsilon = \mu = n$ and PL modes supported by PIM-2 with $\varepsilon = \mu = n$; they coincide exactly. On the basis of the dispersion relationships in Figs. 1(c) and (d), Table 1 summarizes all the possible CPA and laser modes in PIMs with $\varepsilon = \mu = n$, which are classified into three cases. In the first case, the CPA and laser modes appear under different conditions (see the green area in Table 1), i.e., with different β. In the second case, the CPA and laser modes appear simultaneously (see the orange area in Table 1), i.e., with the same β. In the third case, the PA or PL mode occurs in a PIM slab with a lower refractive index for incident angles beyond its critical angle (see the blue area in Table 1). Such cases will be successively employed to study the scenario in Fig. 1(b).

3 Numerical demonstration of negative refraction in PIMs ($\varepsilon = \mu$)

First, we illustrate the negative refraction effect for the case in which the CPA and laser modes appear under dif-

Table 1 The CPA and laser modes in PIMs ($\varepsilon = \mu = n$) with different parameters for TE polarization.

Index(n)	$0 < n < 1$				$n = 1$	$n > 1$		
Modes / Materials	$\beta = 0$	$\beta \neq 0$			$\beta \neq 0$	$\beta = 0$	$\beta \neq 0$	
		β_1	β_2	$\theta > \theta_c$			β_1	β_2
PIM-1	CPA & Laser	CPA	Laser	PA	CPA & Laser	CPA & Laser	CPA	Laser
PIM-2	CPA & Laser	Laser	CPA	PL	CPA & Laser	CPA & Laser	Laser	CPA

ferent conditions by using COMSOL Multiphysics. We take $n = 1.5$ as an example. Both the PIM-1 and PIM-2 slabs have the same thickness, $d = 2\lambda$, and are placed on the left and right sides of an air gap with $l = 3\lambda$. On the basis of Fig. 1(c), for the PIM-1 slab, $\beta_{cpa}^{(1)} = 0.577k_0$ is chosen for the CPA mode, and $\beta_{laser}^{(1)} = 0.627k_0$ is chosen for the laser mode; for the PIM-2 slab, $\beta_{laser}^{(2)} = 0.577k_0$ is chosen to obtain the laser mode, and $\beta_{cpa}^{(2)} = 0.627k_0$ is chosen to realize the CPA mode. Now we consider that a TE plane wave strikes this system from air. For left incidence with $\theta = 35.20°$ (i.e., $\beta_{in} = 0.577k_0$), CPA and laser modes can function exactly in the PIM-1 and PIM-2 slabs, respectively. As a result, perfect negative refraction with backward energy flow (see the black arrows) can be realized in the air gap, which is numerically verified in Fig. 2(a). For right incident waves with $\theta = 35.20°$, as the angle does not exactly match the required incident angle, $\theta = 38.80°(\beta_{in} = 0.627k_0)$ for obtaining the CPA mode for PIM-2, but is close to this angle, imperfect CPA and laser modes operate in PIM-2 and PIM-1, respectively. Consequently, negative refraction with some scattering occurs, as shown in Fig. 2(b), where backward energy flow still occurs in the air gap. Likewise, for incident waves with $\theta = 38.80°$, negative refraction with scattering appears for waves incident from the left side [see Fig. 2(c)], and perfect negative refraction is observed for right incidence [see Fig. 2(d)]. Therefore, for PIMs in which the CPA and laser modes occur under different conditions, perfect negative refraction can occur for waves coming from one side, whereas negative refraction with some scattering appears for waves incident from the other side. Such scattering is proportional to the momentum deviation of the CPA and laser modes in the PIMs.

Second, we discuss negative refraction by PIMs in which the CPA and laser modes appear simultaneously. Under this condition, only two identical PIMs are required to realize negative refraction, as the CPA and laser modes coexist in the PIMs. We choose PIM-1 to explore negative refraction, and a similar effect can be obtained by using PIM-2. On the basis of Eq. (1), we can derive the coexistence condition for the CPA and laser modes in the PIM-1 slab [33], which is $\eta_1 = k_x\mu_1/k_{1x} =$ i. After some simplifications, this condition can be further given as $\beta_{cpa/laser} = 0$ or $n_{cpa/laser} = 1$ (see the orange area in Table 1). For $\beta_{cpa/laser} = 0$, there exist a series of $n_{cpa/laser}$ values that yield simultaneous realization of the CPA and laser modes, which are given by $n_{cpa/laser}k_0d = \pi/2 + N\pi$ [33, 34], where N is a positive integer. For $n_{cpa/laser} = 1$, there are a series of $\beta_{cpa/laser} \neq 0$ values for the coexistence of the CPA and laser modes, which can be deduced from $(1 - \beta_{cpa/laser}^2)^{1/2}k_0d = \pi/2 + N\pi$ [33, 34]. To clearly

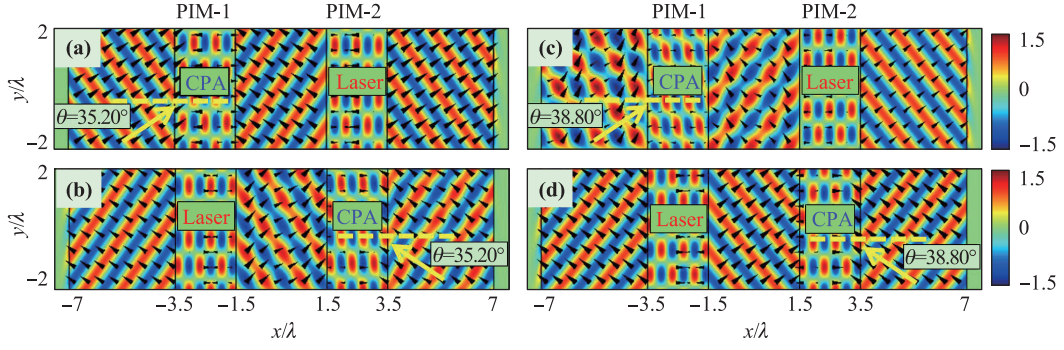

Fig. 2 The simulated electric field patterns for negative refraction using a pair of PIMs ($\varepsilon = \mu = n$) with CPA and laser modes occurring in different conditions. **(a)** and **(b)** are the simulated electric field patterns for the incident waves with $\theta = 35.20°$ from the left and right sides, respectively. **(c)** and **(d)** are the simulated electric field patterns for the incident waves with $\theta = 38.80°$ from the left and right sides, respectively. In all plots, $\varepsilon = \mu = n = 1.5$ is set for both PIM-1 and PIM-2. The thickness of both PIM-1 and PIM-2 are $d = 2\lambda$, and the distance between these two PIMs is $l = 3\lambda$.

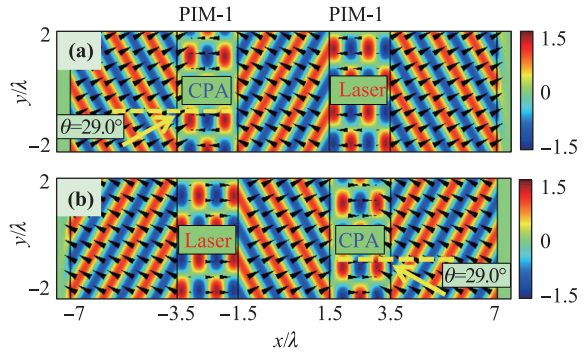

Fig. 3 The simulated electric field patterns for negative refraction using PIM-1 ($\varepsilon = \mu = n$) with CPA and laser modes occurring at the same condition. **(a)** and **(b)** are the simulated electric field patterns for incident waves with $\theta = 29°$ from the left and right sides, respectively. $n = 1$ is set for PIM-1.

demonstrate negative refraction, we choose the case of $n_{cpa/laser} = 1$ and consider two identical PIM-1 slabs in the configuration shown in Fig. 1(b). As shown in Fig. 1(c), for the PIM-1 slab with $d = 2\lambda$, one solution for obtaining the CPA and laser modes concurrently is $\beta_{cpa/laser} = 0.485k_0$. To match this wavevector, a TE plane wave at $\theta = 29.0°$ is incident from air into the PIM-1 system, as shown in Figs. 3(a) and (b), where perfect bidirectional negative refraction occurs, with backward energy flow appearing in the air gap. Therefore, when the CPA and laser modes function simultaneously in a PIM slab, perfect bidirectional negative refraction can be realized by using a pair of identical PIMs. Unlike those in Fig. 2, which meet PT symmetry, here the left and right PIMs are identical and symmetric, and the wave propagation is reciprocal.

Third, we investigate negative refraction for the PA and PL modes in PIMs with a lower refractive index. Without loss of generality, $n = 0.5$ is chosen for the PIMs to achieve the PA and PL modes. On the basis of Eqs. (2) and (3), the PA mode for PIM-1 and the PL mode for PIM-2 are obtained by using the same tangential momentum, i.e., $\beta_{pa/pl} = 0.6847k_0$. Waves incident at $\theta = 39.23°$ (which exactly matches $\beta_{pa/pl} = 0.6847k_0$) from the left side experience a dissipative process in PIM-1 without any reflection (the PA mode operates in PIM-1). Next, the transmitted wave with near zero amplitude in the air gap is enhanced symmetrically in PIM-2 (the PL mode operates in PIM-2). This dissipation and enhancement process is well illustrated in Fig. 4(a). Furthermore, as shown in the inset in Fig. 4(a), the negative refraction disappears. For right incidence with $\theta = 39.23°$, waves will perfectly undergo an enhanced and then dissipative process in PIM-2 and PIM-1 respectively [see Fig. 4(b)]. Negative refraction with backward energy flow also disappears, and the field in the air gap is strongly enhanced [see the inset in Fig. 4(b)]. Therefore, for PIMs with a lower refractive index, negative refraction will disappear for both incident directions. Instead, there is an asymmetric field amplitude [37] in the air gap. Physically, it stems from the disappearance of the CPA and laser modes, so the channel of backward energy flow cannot be established. In addition, as the dissipation and amplification coefficients of the PA and PL modes are the same, perfect total transmission without any reflection occurs for both incident directions.

4 Negative refraction and planar focusing in PIMs ($\varepsilon \neq \mu$) with subwavelength thickness

In the above discussions, as a demonstration of the fundamental principle, PIMs ($\varepsilon = \mu$) with a larger thickness ($d = 2\lambda$) are employed to realize some interesting phe-

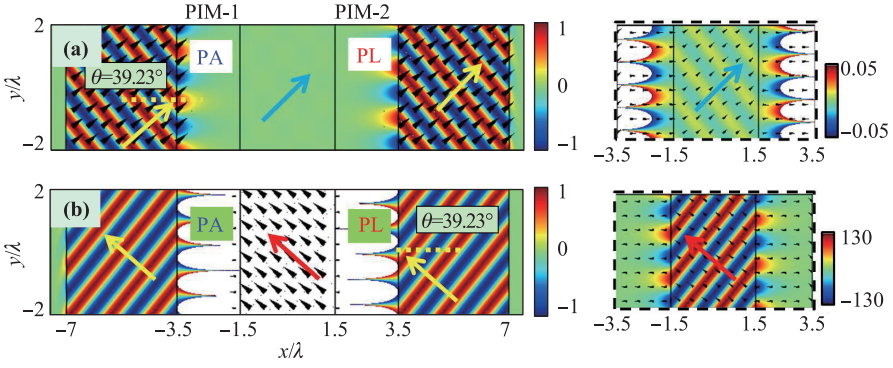

Fig. 4 The simulated electric field patterns for PA and PL modes in PIMs ($\varepsilon = \mu = n$) with a lower refractive index. **(a)** and **(b)** are the simulated electric field patterns for the incident waves with $\theta = 39.23°$ from the left and right sides, respectively. $n = 0.5$ is set for both PIMs. The insets are the related field patterns from $x = -3.5\lambda$ to $x = 3.5\lambda$ ($y = -2\lambda$ to $y = 2\lambda$) and the arrows in the insets denote the directions of energy flow in the air gaps. In plots, the white areas indicate the electric fields are beyond the color bars.

nomena. In fact, even for PIMs ($\varepsilon = \mu$) with subwavelength thickness, except for PIMs with lower refractive index, results similar to those above can be obtained as well, but at the price of a higher n in the PIMs. As we have demonstrated previously that CPA and laser modes with $\beta_{cpa/laser} \neq 0$ appear simultaneously only for PIMs with $n = 1$, the concurrent condition of CPA and laser modes with $\beta_{cpa/laser} \neq 0$ is not available for PIMs ($\varepsilon = \mu$) with subwavelength thickness. Consequently, negative refraction could not be realized with a pair of identical subwavelength PIM slabs. To solve this problem, in the following we will employ PIMs with $\varepsilon \neq \mu$ to explore negative refraction in subwavelength PIM slabs. As there is no need for $\varepsilon = \mu$ in PIM-1 ($\varepsilon_1 = -\mathrm{i}\varepsilon$ and $\mu_1 = \mathrm{i}\mu$), this choice can increase the parameter freedom for Eq. (1). Consequently, the CPA and laser modes with $\beta_{cpa/laser} \neq 0$ might be realized simultaneously in a subwavelength PIM-1 ($\varepsilon \neq \mu$) slab. For example, the subwavelength scale is assumed as $d = 0.1\lambda$, and $\beta_{cpa/laser} = 0.5k_0$ is chosen for realizing the CPA and laser modes concurrently. By solving Eq. (1), $\varepsilon = 2.253$ and $\mu = 2.88$ are found to be among several solutions that realize the coexistence of the CPA and laser modes in PIM-1. Here we use PIM-1 with these parameters to verify the occurrence of negative refraction in the structure in Fig. 1(b), where the distance between the PIM-1 slabs is $l = 3\lambda$. The corresponding electric field patterns for left and right incidence are shown in Figs. 5(a) and (b), respectively, where perfect negative refraction with backward energy flow appears in both cases. When other appropriate parameters of the PIM-1 slabs are applied, perfect bidirectional negative refraction with the desired refraction angle can be realized as well. Therefore, if we engineer PIM-1 slabs with well-defined profiles to obtain the CPA and laser modes simultaneously, wide-angle negative refraction can be achieved for planar focusing [26, 36]. For example, the focus length is set to $f = 6\lambda$, and two PIM-1 slabs with $d = 0.1\lambda$ are placed at $x = -6\lambda$ and $x = 6\lambda$. Each slab with a length of 15λ is divided into 15 cells, and each cell with a length of λ is marked with positions from $N = -7$ to $N = 7$ from bottom to top (see the schematic configuration of 15 cells on the right side of Fig. 5). Accordingly, the required tangential momentum for realizing the CPA and laser modes simultaneously in each cell is given as $\beta_N = k_0 N\lambda/(f^2 + N^2\lambda^2)^{1/2}$. As a result, well-defined profiles of PIM-1 in each cell can be obtained by employing Eq. (1) and β_N. For a pair of PIM-1 slabs with these profiles, the simulated electric field patterns for planar focusing are shown in Figs. 5(c) and (d), where the point sources are located at $(-12\lambda, 0)$ and $(12\lambda, 0)$, respectively. There are apparently two focusing points located at $(0, 0)$ and $(12\lambda, 0)$ owing to the wide-angle negative refraction of the point source at $(-12\lambda, 0)$ [see Fig. 5(c)]. Similarly, there are two focusing points at $(0, 0)$ and $(-12\lambda, 0)$ for the point source at $(12\lambda, 0)$ [see Fig. 5(d)]. As these cells can support the CPA and laser modes simultaneously for point sources at these two positions, bidirectional planar focusing, which is not accessible in PT-symmetric systems [26, 36], can be realized. In addition, if the point source deviates slightly from these two locations $(\pm 12\lambda, 0)$, e.g., if the point source is placed at $(11\lambda, \lambda)$, because wide-angle negative refraction can be obtained to some extent, similar planar focusing can be observed. Note that planar focusing by a PT-symmetric system has diffraction-limited imaging resolution because only the propagating wave components can be focused [36]. Therefore, the image resolution of our PIM-1 system also does not break the diffraction limit, as the working principle in the PIM-1 system is the same as that in PT-symmetric systems.

5 Discussion and conclusion

In conclusion, bidirectional negative refraction and planar focusing were well demonstrated in the proposed PIM systems, even for slabs with subwavelength thickness. The underlying physics arises from the coexistence of the CPA and laser modes in the PIMs. Therefore, negative refraction in our PIM systems overcomes the disadvantages of the unidirectional limit in current technologies [26, 36], and loss-free and bidirectional features are revealed. Specifically, in a pair of PIMs with a lower refractive index, an asymmetric field amplitude with perfect total transmission can be observed. In fact, for transverse magnetic (TM) polarization (where the magnetic field is along the z direction), similar results could be obtained. In particular, negative refraction and an asymmetric field amplitude without limitation of the polarization can be realized in PIMs with $\varepsilon = \mu$.

In PT-symmetric systems [26], it is challenging to use these materials for planar focusing in practice, as the permittivities are purely imaginary. However, by designing an omnidirectional CPA in a multilayered structure with conventional lossy materials, planar focusing based on PT symmetry can be realized [36]. Here we acknowledge that although experimental realization of a PIM possessing both loss and gain elements simultaneously by current metamaterial techniques is still relatively challenging, it is not entirely impossible. Two theoretical schemes [31, 32] to realize materials with properties similar to those of PIMs have been proposed recently. For example, PIMs can be effectively mimicked by employing PT-symmetric materials in layered structures [31], and a similar CPA–laser effect can be realized. The PIMs can be well designed by using a core–shell configuration [32], where the loss and gain media are distributed in ei-

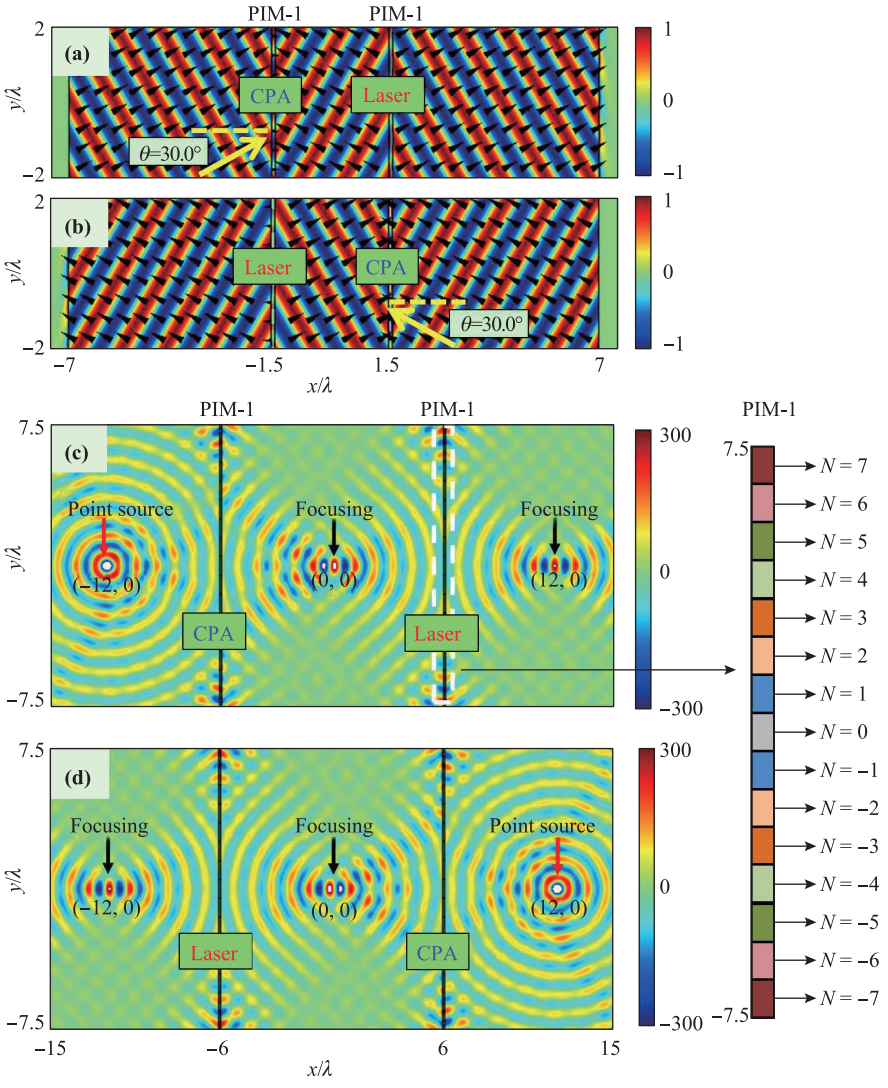

Fig. 5 The simulated electric field patterns for sub-wavelength PIM-1 ($\varepsilon \neq \mu$) with CPA and laser modes occurring simultaneously. **(a)** and **(b)** are the simulated electric field patterns of negative refraction for incident waves with $\theta = 30°$ from the left and right sides, respectively. $\varepsilon = 2.253$ and $\mu = 2.88$ are set for PIM-1 ($\varepsilon_1 = -\mathrm{i}\varepsilon$ and $\mu_1 = \mathrm{i}\mu$). **(c)** and **(d)** are the simulated electric field patterns of planar focusing for the point sources locating at $(-12\lambda, 0)$ and $(12\lambda, 0)$ respectively, where a pair of PIM-1 slabs are equipped with the same well-defined profiles: $\varepsilon = 2.5$ and $\mu = 2.5$ for cells with $N = 0$; $\varepsilon = 2.483$ and $\mu = 2.534$ for cells with $N = \pm 1$; $\varepsilon = 2.414$ and $\mu = 2.65$ for cells with $N = \pm 2$; $\varepsilon = 2.287$ and $\mu = 2.822$ for cells with $N = \pm 3$; $\varepsilon = 2.126$ and $\mu = 3.1$ for cells with $N = \pm 4$; $\varepsilon = 1.931$ and $\mu = 3.477$ for cells with $N = \pm 5$; $\varepsilon = 1.7$ and $\mu = 4.04$ for cells with $N = \pm 6$; $\varepsilon = 1.425$ and $\mu = 4.937$ for cells with $N = \pm 7$. In (c) and (d), these sub-wavelength PIM slabs are identical, which are composed of 15 cells marked by different colors shown in the right side.

ther the cores or the shells. Another route we suggest is embedding a series of subwavelength 3D particles or 2D cylinders of dielectric gain media in a lossy background medium. For instance, in a waveguide system, one can design a junction consisting of a lossy epsilon-near-zero medium with a dielectric gain cylinder, in which the magnetic resonances of TM waves in this cylinder cavity can induce an effective permeability with a negative imaginary part [28]; therefore, appropriate tuning of the geometric and material parameters can lead to a PIM with near-zero index. On the other hand, great progress has been made recently in optical gain media [38] experimentally, offering the potential for the realization of PIMs in the future.

Acknowledgements This work was supported by the National Natural Science Foundation of China (Grant No. 11604229), the Natural Science Foundation of Jiangsu Province (Grant No. BK20171206), the Postdoctoral Science Foundation of China (Grant No. 2015M580456), and the Fundamental Research Funds

for the Central Universities (Grant No. 20720170015). Y. Xu is grateful for support from the Collaborative Innovation Center of Suzhou Nano Science and Technology at Soochow University.

References

1. V. G. Veselago, The electrodynamics of substances with simultaneously negative values of ε and m, *Sov. Phys. Usp.* 10(4), 509 (1968)
2. J. B. Pendry, Negative refraction makes a perfect lens, *Phys. Rev. Lett.* 85(18), 3966 (2000)
3. S. Xi, H. Chen, T. Jiang, L. Ran, J. Huangfu, B. I. Wu, J. A. Kong, and M. Chen, Experimental verification of reversed Cherenkov radiation in left-handed metamaterial, *Phys. Rev. Lett.* 103(19), 194801 (2009)
4. P. R. Berman, Goos–Hänchen shift in negatively refractive media, *Phys. Rev. E* 66(6), 067603 (2002)
5. R. A. Shelby, D. R. Smith, and S. Schultz, Experimental verification of a negative index of refraction, *Science* 292(5514), 77 (2001)
6. A. J. Hoffman, L. Alekseyev, S. S. Howard, K. J. Franz, D. Wasserman, V. A. Podolskiy, E. E. Narimanov, D. L. Sivco, and C. Gmachl, Negative refraction in semiconductor metamaterials, *Nat. Mater.* 6(12), 946 (2007)
7. J. Yao, Z. Liu, Y. Liu, Y. Wang, C. Sun, G. Bartal, A. M. Stacy, and X. Zhang, Optical negative refraction in bulk metamaterials of nanowires, *Science* 321(5891), 930 (2008)
8. S. Zhang, Y. Park, J. Li, X. Lu, W. Zhang, and X. Zhang, Negative refractive index in chiral metamaterials, *Phys. Rev. Lett.* 102(2), 023901 (2009)
9. C. Luo, S. G. Johnson, J. D. Joannopoulos, and J. B. Pendry, All-angle negative refraction without negative effective index, *Phys. Rev. B* 65(20), 201104 (2002)
10. E. Cubukcu, K. Aydin, E. Ozbay, S. Foteinopoulou, and C. M. Soukoulis, Negative refraction by photonic crystals, *Nature* 423(6940), 604 (2003)
11. Y. Xie, W. Wang, H. Chen, A. Konneker, B. Popa, and S. A. Cummer, Wavefront modulation and subwavelength diffractive acoustics with an acoustic metasurface, *Nat. Commun.* 5, 5553 (2014)
12. Y. Xu, Y. Fu, and H. Chen, Steering light by a subwavelength metallic grating from transformation optics, *Sci. Rep.* 5(1), 12219 (2015)
13. S. Maslovski and S. Tretyakov, Phase conjugation and perfect lensing, *J. Appl. Phys.* 94(7), 4241 (2003)
14. P. Chen and A. Alù, Subwavelength imaging using phase-conjugating nonlinear nanoantenna arrays, *Nano Lett.* 11(12), 5514 (2011)
15. J. B. Pendry, Time reversal and negative refraction, *Science* 322(5898), 71 (2008)
16. S. Palomba, S. Zhang, Y. Park, G. Bartal, X. Yin, and X. Zhang, Optical negative refraction by four-wave mixing in thin metallic nanostructures, *Nat. Mater.* 11(1), 34 (2012)
17. Z. Lin, H. Ramezani, T. Eichelkraut, T. Kottos, H. Cao, and D. N. Christodoulides, Unidirectional invisibility induced by PT-symmetric periodic structures, *Phys. Rev. Lett.* 106(21), 213901 (2011)
18. S. Longhi, PT-symmetric laser absorber, *Phys. Rev. A* 82(3), 031801 (2010)
19. Y. D. Chong, L. Ge, and A. D. Stone, Coherent perfect absorbers: Time-reversed lasers, *Phys. Rev. Lett.* 106, 093902 (2011)
20. Y. Sun, W. Tan, H. Q. Li, J. Li, and H. Chen, Experimental demonstration of a coherent perfect absorber with PT phase transition, *Phys. Rev. Lett.* 112(14), 143903 (2014)
21. X. Zhu, L. Feng, P. Zhang, X. Yin, and X. Zhang, One-way invisible cloak using parity-time symmetric transformation optics, *Opt. Lett.* 38(15), 2821 (2013)
22. X. Zhu, Y. Peng, and D. Zhao, Anisotropic reflection oscillation in periodic multilayer structures of parity-time symmetry, *Opt. Express* 22(15), 18401 (2014)
23. X. Zhu, Defect states and exceptional point splitting in the band gaps of one-dimensional parity-time lattices, *Opt. Express* 23(17), 22274 (2015)
24. Y. Fu, Y. Xu, and H. Y. Chen, Zero index metamaterials with PT symmetry in a waveguide system, *Opt. Express* 24(2), 1648 (2016)
25. Y. Wu, B. Zhu, S. F. Hu, Z. Zhou, and H. Zhong, Floquet control of the gain and loss in a PT-symmetric optical coupler, *Front. Phys.* 12(1), 121102 (2017)
26. R. Fleury, D. L. Sounas, and A. Alù, Negative refraction and planar focusing based on parity-time symmetric metasurfaces, *Phys. Rev. Lett.* 113(2), 023903 (2014)
27. X. Zhu, H. Ramezani, C. Shi, J. Zhu, and X. Zhang, PT-symmetric acoustics, *Phys. Rev. X* 4(3), 031042 (2014)
28. Y. Fu, X. Zhang, Y. Xu, and H. Chen, Design of zero index metamaterials with PT symmetry using epsilon-near-zero media with defects, *J. Appl. Phys.* 121(9), 094503 (2017)
29. D. Dragoman, Complex conjugate media: Alternative configurations for miniaturized lasers, *Opt. Commun.* 284(8), 2095 (2011)
30. A. Basiri, I. Vitebskiy, and T. Kottos, Light scattering in pseudopassive media with uniformly balanced gain and loss, *Phys. Rev. A* 91(6), 063843 (2015)
31. S. Xiao, J. Gear, S. Rotter, and J. Li, Effective PT-symmetric metasurfaces for subwavelength amplified sensing, *New J. Phys.* 18(8), 085004 (2016)
32. P. Bai, K. Ding, G. Wang, J. Luo, Z. Zhang, C. T. Chan, Y. Wu, and Y. Lai, Simultaneous realization of a coherent perfect absorber and laser by zero-index media with both gain and loss, *Phys. Rev. A* 94(6), 063841 (2016)

33. Y. Xu, Y. Fu, and H. Chen, Electromagnetic wave propagations in conjugate metamaterials, *Opt. Express* 25(5), 4952 (2017)

34. Y. Fu, Y. Cao, S. A. Cummer, Y. Xu, and H. Chen, Coherent perfect absorber and laser modes in purely imaginary metamaterials, *Phys. Rev. A* 96(4), 043838 (2017)

35. Y. Fu, Y. Xu, H. Chen, and S. A. Cummer, Coherent perfect absorption and laser modes in a cylindrical structure of conjugate metamaterials, *New J. Phys.* 20(1), 013015 (2018)

36. F. Monticone, C. A. Valagiannopoulos, and A. Alù, Parity-time symmetric nonlocal metasurfaces: All-angle negative refraction and volumetric imaging, *Phys. Rev. X* 6(4), 041018 (2016)

37. Y. Fu and Y. Xu, Asymmetric effects in waveguide systems using PT symmetry and zero index metamaterials, *Sci. Rep.* 7(1), 12476 (2017)

38. Z. J. Wong, Y. L. Xu, J. Kim, K. O'Brien, Y. Wang, L. Feng, and X. Zhang, Lasing and anti-lasing in a single cavity, *Nat. Photonics* 10(12), 796 (2016)